Inorg. Chem. **2006**, *45*, 752−760

Complexes of Cytotoxic Chelators from the Dipyridyl Ketone Isonicotinoyl Hydrazone (HPKIH) Analogues

Paul V. Bernhardt,*,† Johan Mattsson,† and Des R. Richardson*,‡

Centre for Metals in Biology, Department of Chemistry, University of Queensland, Brisbane 4072, Australia, and Children's Cancer Institute Australia for Medical Research, Iron Metabolism and Chelation Program, PO Box 81, High St, Randwick, Sydney 2031, Australia

Received September 14, 2005

In an effort to better understand the antiproliferative effects of the tridentate hydrazone chelators di-2-pyridyl ketone isonicotinoyl hydrazone (HPKIH) and di-2-pyridyl ketone benzoyl hydrazone (HPKBH), we report the coordination chemistry of these ligands with the divalent metal ions, Mn, Co, Ni, Cu, and Zn. These complexes are compared with their Fe^{II} analogues which were reported previously. The crystal structures of $Co(PKIH)_2$, $Ni(PKIH)_2$, $Cu(PKIH)_2$, $Mn(PKBH)_2$, $Ni(PKBH)_2$, $Cu(PKBH)_2$, and $Zn(PKBH)_2$ are reported where similar bis-tridenate coordination modes of the ligands are defined. In pure DMF, all complexes except the Zn^{II} compounds exhibit metal-centered $M^{III/II}$ (Mn, Fe, Co, Ni) or $M^{II/I}$ (Cu) redox processes. All complexes show ligand-centered reductions at low potential. Electrochemistry in a mixed water/DMF solvent only elicited metal-centered responses from the Co and Fe complexes. Remarkably, all complexes show antiproliferative activity against the SK-N-MC neuroepithelioma cell line similar to (HPKIH) or significantly greater than that of the (HPKBH) ligand which suggests a mechanism that does not only involve the redox activity of these complexes. In fact, we suggest that the complexes act as lipophilic transport shuttles that allow entrance to the cell and enable the delivery of both the ligand and metal which act in concert to inhibit proliferation.

Introduction

Iron is essential to almost all forms of life. In humans it is found at the active site of a number of key proteins involved in oxygen transport, metabolism, and respiration in addition to hydroxylating enzymes, lipoxygenases, cycloxygenases, and the rate-limiting enzyme of DNA synthesis, ribonucleotide reductase (RR).[1] Rapidly growing neoplastic cells such as neuroblastoma and leukemia have a particularly high demand for Fe, and these characteristics render this metal ion a potential therapeutic target for preventing tumor cell proliferation.[1−4] As an example, desferrioxamine (DFO, Figure 1), the most commonly used drug to treat Fe overload, has also shown activity against tumor growth in human[5,6] and animal studies.[7]

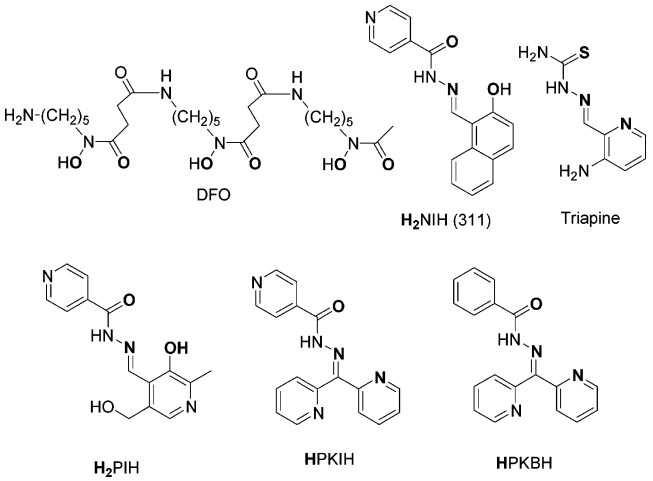

Figure 1. Line drawings of the chelators discussed in this work. Donor atoms in bold type.

Although Fe is often associated with redox reactions as part of its biological role (e.g., cytochromes), the antiproliferative effects of Fe chelators may occur in various ways

* To whom correspondence should be addressed. E-mail: P.bernhardt@uq.edu.au.
† University of Queensland.
‡ Children's Cancer Institute Australia for Medical Research.

(1) Tam, T. F.; Leung-Toung, R.; Li, W.; Wang, Y.; Karimian, K.; Spino, M. *Curr. Med. Chem.* **2003**, *10*, 983−995.
(2) Lovejoy, D. B.; Richardson, D. R. *Curr. Med. Chem.* **2003**, *10*, 1035−1049.
(3) Buss, J. L.; Torti, F. M.; Torti, S. V. *Curr. Med. Chem.* **2003**, *10*, 1021−1034.
(4) Le, N.; Richardson, D. *Biochim. Biophys. Acta* **2002**, *1603*, 31.
(5) Becton, D. L.; Roberts, B. *Cancer. Res.* **1989**, *49*, 4809−4812.

10.1021/ic051573l CCC: $33.50
Published on Web 12/08/2005

that may or may not involve electron-transfer reactions. Nevertheless, the formation of an Fe complex within the cell is assumed to be a common theme. The sites at which a chelator may acquire Fe (and in what form) are difficult to establish. There are several intracellular sites at which Fe in either its di- or trivalent oxidation state may be intercepted during its transport via the serum protein transferrin to its destination in storage proteins such as ferritin or at the active sites of heme- and non-heme-containing proteins.[2,4]

Intracellular Fe depletion through interaction with Fe-specific chelators has been found to affect the expression of important molecules involved in cell-cycle progression.[4,8,9] From a simple perspective, Fe depletion may occur if a high intracellular concentration of chelator can be established to the point where the total amount of Fe within the cell is lowered. This may include the attack of specific Fe-protein active sites. The marked cytotoxicity of the tridentate hydrazone, H_2NIH (also known as 311), is strongly linked with Fe complexation.[10−13] It forms a six-coordinate 1:2 Fe^{III}/ligand complex that cannot be reduced at a physiologically relevant potential.[10] That is, the high antiproliferative activity of H_2NIH (in complexation with intracellular Fe) cannot result from redox chemistry.[10,11] The antiproliferative activity of H_2NIH was lost completely when complexed with Fe^{III} prior to its introduction to cell culture,[10] which suggests that the activity of this chelator is related to its ability to deplete key proteins of Fe upon entering the cell.

The redox activity of Fe may be exploited against cancer cells in an effort to produce potentially cytotoxic reactive oxygen species (ROS).[14] The Fenton reaction involves the Fe^{II}-catalyzed decomposition of hydrogen peroxide to generate highly reactive hydroxyl free radicals. More than 100 years after it was originally reported,[15] the mechanism of this complex reaction is still controversial,[16] but it is accepted that the reaction is initiated by the oxidation of an Fe^{II} complex by hydrogen peroxide and that hydroxyl free radicals are produced as one of many products. Chelators that form redox-active Fe complexes within the cell may be implicated in the generation in vivo of potentially cytotoxic ROS.[17,18] The well-known anticancer drug bleomycin, when complexed with Fe^{II}, is a potent generator of Fenton-mediated hydroxyl radicals.[19,20] One potential Fe chelator that is currently in Phase II trials as an anticancer drug is the thiosemicarbazone, Triapine.[21−27] Although its Fe coordination chemistry has not been explored in detail, it has been shown to be capable of catalyzing Fenton chemistry in the presence of Fe and hydrogen peroxide.[11]

Recently, we investigated the chemistry and antiproliferative activity of a new series of chelators based on 2-pyridinecarbaldehyde isonicotinoyl hydrazone (HPKIH).[18,28,29] In an extensive investigation of the Fe coordination chemistry of these chelators, we established that, like many of the other ligands discussed above, the chelators undergo deprotonation of their NH group upon complexation with Fe and readily form a six-coordinate 1:2 Fe/ligand complex.[29] However, the complexes of the HPKIH series are interesting in that our electrochemical and spectroscopic studies have firmly established that air-stable divalent Fe complexes are formed,[29] whereas the trivalent oxidation state is preferred for complexes of other biologically active chelators such as DFO and H_2NIH. An interesting feature of our investigations is that the cytotoxicity of complexes of the HPKIH free ligands is not inhibited by precomplexation (in situ) with Fe.[28] This implies that intracellular Fe depletion or competitive removal of Fe from the active sites of key proteins cannot be totally associated with the antiproliferative activity of the HPKIH chelators. In fact, this suggests that complexation with Fe may lead to the generation of a complex that mediates cytotoxicity, perhaps by redox cycling.[18,28,29] To test this hypothesis, we report the coordination chemistry and electrochemistry of the divalent Mn, Co, Ni, Cu, and Zn complexes of the two representative members of this family, namely, HPKIH and the benzoyl hydrazone analogue, HPKBH. As we will demonstrate, the cytotoxicity of these complexes is comparable with or greater than that shown by the free ligand and the Fe^{II} complexes. This investigation sheds new light on the possible mechanisms of action of these complexes, and we suggest that mechanisms in addition to redox activity are involved in the antiproliferative efficacy of these compounds.

Experimental Section

Syntheses. The di-2-pyridyl ketone isonicotinoyl hydrazone (HPKIH) and di-2-pyridyl ketone benzoyl hydrazone (HPKBH)

(6) Donfrancesco, A.; Deb, G.; Dominici, C.; Pileggi, D.; Castello, M. A.; Helson, L. *Cancer. Res.* **1990**, *50*, 4929−4930.
(7) Jiang, X. P.; Wang, F.; Yang, D. C.; Elliott, R. L.; Head, J. F. *Anticancer Res.* **2002**, *22*, 2685−2692.
(8) Gao, J.; Richardson, D. R. *Blood* **2001**, *98*, 842−850.
(9) Kicic, A.; Chua, A. C.; Baker, E. *Cancer* **2001**, *92*, 3093−3110.
(10) Richardson, D. R.; Bernhardt, P. V. *J. Biol. Inorg. Chem.* **1999**, *4*, 266−273.
(11) Chaston, T. B.; Lovejoy, D. B.; Watts, R. N.; Richardson, D. R. *Clin. Cancer Res.* **2003**, *9*, 402−414.
(12) Richardson, D. R.; Tran, E. H.; Ponka, P. *Blood* **1995**, *86*, 4295−4306.
(13) Richardson, D. R.; Milnes, K. *Blood* **1997**, *89*, 3025−3038.
(14) Chaston, T. B.; Richardson, D. R. *Am. J. Hematol.* **2003**, *73*, 200−210.
(15) Fenton, H. J. H. *J. Chem. Soc.* **1894**, 899−910.
(16) Dunford, H. B. *Coord. Chem. Rev.* **2002**, *233*−*234*, 311−318.
(17) Yuan, J.; Lovejoy, D. B.; Richardson, D. R. *Blood* **2004**, *104*, 1450−1458.
(18) Chaston, T. B.; Watts, R. N.; Yuan, J.; Richardson, D. R. *Clin. Cancer Res.* **2004**, *10*, 7365−7374.
(19) Burger, R. M. *Structure Bond.* **2000**, *97*, 287−323.
(20) Boger, D. L.; Cai, H. *Angew. Chem., Int. Ed.* **1999**, *38*, 448−476.
(21) Li, J.; Chen, S.-H.; Li, X.; Niu, C.; Doyle, T. W. *Tetrahedron* **1998**, *54*, 393−400.
(22) Finch, R. A.; Liu, M. C.; Cory, A. H.; Cory, J. G.; Sartorelli, A. C. *Adv. Enzymol. Regul.* **1999**, *39*, 3−12.
(23) Li, J.; Zheng, L.-M.; King, I.; Doyle, T. W.; Chen, S.-H. *Front. Biotechnol. Pharm.* **2000**, *1*, 314−335.
(24) Li, J.; Zheng, L.-M.; King, I.; Doyle, T. W.; Chen, S.-H. *Curr. Med. Chem.* **2001**, *8*, 121−133.
(25) Feun, L.; Modiano, M.; Lee, K.; Mao, J.; Marini, A.; Savaraj, N.; Plezia, P.; Almassian, B.; Colacino, E.; Fischer, J.; MacDonald, S. *Cancer Chemother. Pharmacol.* **2002**, *50*, 223−229.
(26) Wadler, S.; Makower, D.; Clairmont, C.; Lambert, P.; Fehn, K.; Sznol, M. *J. Clin. Oncol.* **2004**, *22*, 1553−1563.
(27) Yen, Y.; Margolin, K.; Doroshow, J.; Fishman, M.; Johnson, B.; Clairmont, C.; Sullivan, D.; Sznol, M. *Cancer Chemother. Pharmacol.* **2004**, *54*, 331−342.
(28) Becker, E. M.; Lovejoy, D. B.; Watts, R. N.; Richardson, D. R. *Br. J. Pharmacol.* **2003**, *138*, 819−830.
(29) Bernhardt, P. V.; Caldwell, L. M.; Chaston, T. B.; Chin, P.; Richardson, D. R. *J. Biol. Inorg. Chem.* **2003**, *8*, 866−880.

ligands were prepared as described.[29] The $Fe(PKIH)_2$ and $Fe(PKBH)_2$ complexes were also prepared using published procedures.[29]

General Synthesis of $M(PKIH)_2$ (M = Mn, Co, Ni, Cu, Zn) Complexes. Et_3N (140 μL, 1.0 mmol) was added to a suspension of HPKIH (0.3 g, 1.0 mmol) in EtOH (50 mL), and the suspension dissolved after warming. A solution containing 0.5 mmol of the appropriate divalent metal salt (see below) in water (50 mL) was added, and the mixture was refluxed for 4 h. The reaction mixture was allowed to cool; then it was transferred to a beaker to allow slow evaporation of the solvent over several days. The solid that formed upon concentration was filtered off and air-dried. Recrystallization details for each compound are given below. The yields of pure complex were in the range of 30−50%.

$[Mn(PKIH)_2]\cdot 2H_2O$. $MnCl_2\cdot 4H_2O$ was used. Red-brown product. Anal. Calcd for $C_{34}H_{24}MnN_{10}O_2\cdot 2H_2O$: C, 58.7; H, 4.1; N, 20.1. Found: C, 58.3; H, 3.6; N, 19.9. IR (KBr, cm^{-1}): $\bar{\nu}$ 1598 m, 1568 s, 1496 vs, 1459 vs, 1436 m, 1363 vs, 1330 s, 1309 s, 1151 m, 1074 vs, 689 m. Electronic spectrum (CH_2Cl_2): λ_{max} (ϵ) 390 (31 700), 276 nm (78 400 M^{-1} cm^{-1}).

$[Co(PKIH)_2]\cdot 2H_2O$. $CoCl_2\cdot 6H_2O$ was used. Brown product. Anal. Calcd for $C_{34}H_{24}CoN_{10}O_2\cdot 2H_2O$: C, 58.4; H, 4.0; N, 20.0. Found: C, 59.3; H, 4.1; N, 19.9. IR (KBr, cm^{-1}): $\bar{\nu}$ 1599 m, 1567 s, 1488 vs, 1454 vs, 1436 m, 1365 vs, 1329 s, 1307 s, 1148 m, 1076 vs, 690 m. Electronic spectrum (CH_2Cl_2): λ_{max} (ϵ) 531 (1100), 385 (45 200), 282 nm (33 700 M^{-1} cm^{-1}). Dark brown X-ray quality crystals were obtained directly from the reaction mixture.

$[Ni(PKIH)_2]\cdot 2H_2O$. $NiCl_2\cdot 6H_2O$ was used. Brown product. Anal. Calcd for $C_{34}H_{24}N_{10}NiO_2\cdot 2H_2O$: C, 58.4; H, 4.0; N, 20.0. Found: C, 58.0; H, 3.9; N, 19.5. IR (KBr, cm^{-1}): $\bar{\nu}$ 1596 m, 1570 s, 1499 vs, 1490 vs, 1457 vs, 1437 m, 1363 vs, 1328 s, 1307 s, 1147 m, 1085 vs, 693 m. Electronic spectrum (CH_2Cl_2): λ_{max} (ϵ) 848 (40), 404 (16 600), 282 nm (15 300 M^{-1} cm^{-1}). Dark brown X-ray quality crystals were obtained directly from the reaction mixture.

$[Cu(PKIH)_2]\cdot 2H_2O$. $CuCl_2\cdot 2H_2O$ was used. Brown product. Anal. Calcd for $C_{34}H_{24}CuN_{10}O_2\cdot 2H_2O$: C, 58.0; H, 4.0; N, 19.9. Found: C, 58.3; H, 3.8; N, 19.8. IR (KBr, cm^{-1}): $\bar{\nu}$ 1599 m, 1571 s, 1499 vs, 1489 vs, 1458 vs, 1436 m, 1361 vs, 1327 s, 1306 s, 1148 m, 1083 vs, 694 m. Electronic spectrum (CH_2Cl_2): λ_{max} (ϵ) 698 (73), 396 (16 000), 274 nm (29 000 M^{-1} cm^{-1}). Dark brown X-ray quality crystals were obtained directly from the reaction mixture.

$Zn(PKIH)_2$. $Zn(NO_3)_2\cdot 6H_2O$ was used. Yellow product. Anal. Calcd for $C_{34}H_{24}N_{10}O_2Zn$: C, 61.0; H, 3.6; N, 20.9. Found: C, 60.2; H, 3.5; N, 20.4. IR (KBr, cm^{-1}): $\bar{\nu}$ 1599 m, 1586 m, 1570 s, 1499 vs, 1488 vs, 1460 vs, 1437 m, 1361 vs, 1326 s, 1306 s, 1148 m, 1085 vs, 692 m. Electronic spectrum (CH_2Cl_2): λ_{max} (ϵ) 389 (28 500), 278 nm (31 000 M^{-1} cm^{-1}).

General Synthesis of $M(PKBH)_2$ (M = Mn, Co, Ni, Cu, Zn) Complexes. Et_3N (140 μL, 1.0 mmol) was added to a suspension of HPKBH (0.3 g, 1.0 mmol) in EtOH (40 mL), and the suspension dissolved after warming. A solution containing 0.5 mmol of the appropriate divalent metal salt (see below) in 50% aqueous EtOH (50 mL) was added, and the mixture was refluxed for 4 h. For the Co^{II} analogue, the reaction mixture was refluxed under nitrogen to minimize oxidation of the complex, and this synthesis was performed in 50% aqueous EtOH. Each reaction mixture was allowed to cool; then it was transferred to a beaker to allow slow evaporation of the solvent over a period of several days. The solid that formed upon concentration of the reaction mixture was filtered off and dried in a vacuum desiccator. Recrystallization details for each compound are given below. The yields were approximately 30−40% after recrystallization.

$Mn(PKBH)_2$. $MnCl_2\cdot 4H_2O$ was used. Red-brown product. Anal. Calcd for $C_{36}H_{26}MnN_8O_2$: C, 65.8; H, 3.9; N, 16.8. Found: C, 65.6; H, 3.9; N, 16.8. IR (KBr, cm^{-1}): $\bar{\nu}$ 1585 s, 1560 m, 1496 vs, 1460 vs, 1434 m, 1360 vs, 1323 s, 1298 s, 1139 m, 1079 vs, 715 vs, 686 s. Electronic spectrum (CH_2Cl_2): λ_{max} (ϵ) 395 (38 800), ~280 (sh, 25 000), 259nm (29 100 M^{-1} cm^{-1}). X-ray quality crystals of $[Mn(PKBH)_2]\cdot CH_2Cl_2$ were obtained by slow evaporation of a 1:1 $MeOH/CH_2Cl_2$ solution of the complex.

$[Co(PKBH)_2]\cdot H_2O$. $CoCl_2\cdot 6H_2O$ was used. Red-brown product. Anal. Calcd for $C_{36}H_{26}CoN_8O_2\cdot H_2O$: C, 63.6; H, 4.2; N, 16.5. Found: C, 63.7; H, 3.9; N, 16.5. IR (KBr, cm^{-1}): $\bar{\nu}$ 1585 s, 1560 m, 1492 vs, 1459 vs, 1434 m, 1363 vs, 1324 vs, 1295 s, 1139 s, 1084 vs, 714 s, 689 s. Electronic spectrum (CH_2Cl_2): λ_{max} (ϵ) 529 (2000), 388 (49 300), 274 nm (47 000 M^{-1} cm^{-1}).

$Ni(PKBH)_2$. $NiCl_2\cdot 6H_2O$ was used. Brown product. Anal. Calcd for $C_{36}H_{26}N_8NiO_2$: C, 65.4; H, 4.0; N, 16.9. Found: C, 65.6; H, 3.9; N, 16.8. IR (KBr, cm^{-1}): $\bar{\nu}$ 1585 s, 1560 m, 1496 vs, 1460 vs, 1434 m, 1360 vs, 1323 s, 1298 s, 1139 m, 1079 vs, 715 vs, 686 s. Electronic spectrum (CH_2Cl_2): λ_{max} (ϵ) 835 (38), 407 (42 900), ~280 (sh, ϵ 39 000), 262 nm (44 500 M^{-1} cm^{-1}). X-ray quality crystals of $[Ni(PKBH)_2]\cdot CH_2Cl_2$ were obtained by slow evaporation of a 1:1 $MeOH/CH_2Cl_2$ solution of the complex.

$Cu(PKBH)_2$. $CuCl_2\cdot 2H_2O$ was used. Brown product. Anal. Calcd for $C_{36}H_{26}CuN_8O_2$: C, 64.9; H, 3.9; N, 16.8. Found: C, 65.1; H, 4.0; N, 16.5. IR (KBr, cm^{-1}): $\bar{\nu}$ 1584 s, 1560 m, 1522 s, 1496 vs, 1460 vs, 1434 m, 1361 vs, 1320 s, 1293 s, 1141 m, 1085 vs, 715 vs, 692 s. Electronic spectrum (CH_2Cl_2): λ_{max} (ϵ) 696 (70), 400 (38 700), ~280 nm (sh, ~33 000 M^{-1} cm^{-1}). Crystals of $[Cu(PKBH)_2]\cdot CH_2Cl_2$ were obtained by slow evaporation of a 1:1 $MeOH/CH_2Cl_2$ solution of the complex but these diffracted weakly. Recrystallization from aqueous EtOH produced X-ray quality crystals of solvent-free $Cu(PKBH)_2$.

$Zn(PKBH)_2$. $ZnSO_4\cdot 5H_2O$ was used. Yellow product. Anal. Calcd for $C_{36}H_{26}N_8O_2Zn$: C, 64.7; H, 3.9; N, 16.8. Found: C, 64.9; H, 3.8; N, 16.6. IR (KBr, cm^{-1}): $\bar{\nu}$ 1586 s, 1560 m, 1499 vs, 1464 vs, 1436 m, 1356 vs, 1323 s, 1290 s, 1141 m, 1086 vs, 720 vs, 687 s. Electronic spectrum (CH_2Cl_2): λ_{max} (ϵ) 394 (37 500), ~280 (sh, 19 000), 258 nm (27 500 M^{-1} cm^{-1}). X-ray quality crystals of $[Zn(PKBH)_2]\cdot CH_2Cl_2$ were obtained by slow evaporation of a 1:1 $MeOH/CH_2Cl_2$ solution of the complex.

Physical Methods. UV−vis spectra were measured on a Analytic Jena Specord instrument as dichloromethane solutions. Infrared spectra were measured on a Perkin-Elmer Model 1600 FT-IR spectrophotometer using KBr disks. Cyclic voltammetry of all complexes was performed with a BAS100B/W electrochemical analyzer employing a glassy carbon working electrode and a platinum wire auxiliary electrode. For nonaqueous experiments, a Ag/Ag^+ (0.01 M in DMF) reference electrode was used. The redox potential of the ferrocene/ferrocenium couple in 100% DMF was +92 mV vs Ag/Ag^+ (0.01 M in DMF). For experiments done in 50% aqueous DMF, an aqueous Ag/AgCl (3 M NaCl) reference electrode was used (E° = 196 mV vs NHE). The supporting electrolyte was 0.1 M Et_4NClO_4, and all solutions were purged with N_2 prior to analysis.

Crystallography. Cell constants at 293 K were determined by a least-squares fit to the setting parameters of 25 independent reflections measured on an Enraf-Nonius CAD4 four-circle diffractometer employing graphite-monochromated Mo Kα radiation (0.71073 Å) and operating in the $\omega-2\theta$ scan mode within the range of $2 < 2\theta < 50$ Å. Data reduction and empirical absorption corrections (ψ scans) were performed with the WINGX suite of

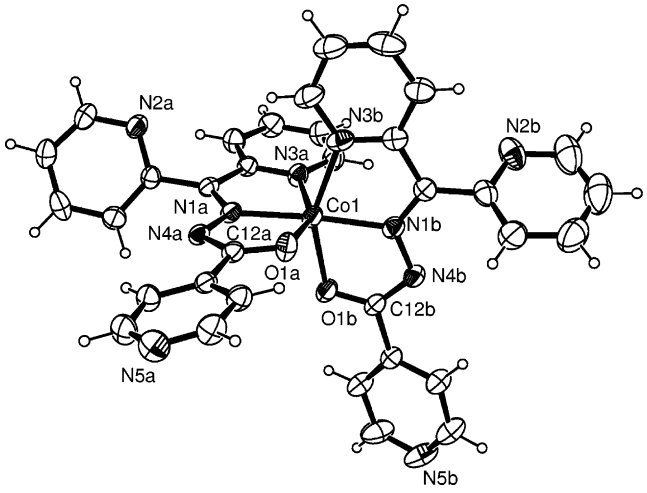

Figure 2. ORTEP drawing of $Co(PKIH)_2$ (30% ellipsoids).

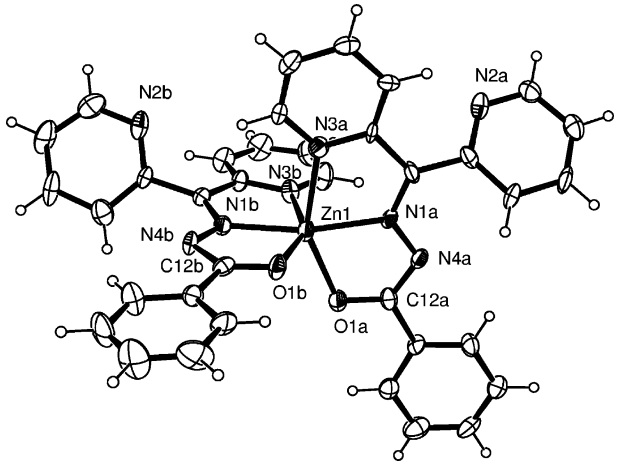

Figure 3. ORTEP view of $Zn(PKBH)_2$ (30% ellipsoids).

programs.[30] Structures were solved by direct methods with SHELXS and refined by full-matrix least-squares analysis with SHELXL-97.[31] All non-H atoms were refined with anisotropic thermal parameters. Aryl and alkyl H atoms were included at estimated positions using a riding model. Water molecules were poorly defined because of the disorder and H-atoms were only located on some O atoms. Molecular structure diagrams (Figures 2 and 3) were produced with ORTEP3.[32] Crystal and refinement data are summarized in Table 1, and selected bond lengths and angles appear in Table 2.

Biological Studies. Cell Culture. The human SK-N-MC neuroepithelioma cell line was obtained from the American Type Culture Collection (ATCC; Rockville, MD). The cells were grown as described[12] and were used to compare these results to those obtained in our previous studies.[12,28]

Effect of the Chelators on Cellular Proliferation. This was examined using the MTT (3-(4,5-dimethylthiazol-2-yl)-2,5-diphenyl tetrazolium) assay as described.[12] MTT color formation was directly proportional to the number of viable cells measured by Trypan blue staining.[12] The results are presented as IC_{50} values, that is, the concentration at which proliferation was inhibited by 50%.

Statistical Analysis. Experimental data were compared using Student's *t*-test. Results were expressed as mean or mean ± SD (number of experiments) and considered statistically significant when $p < 0.05$.

Results and Discussion

The syntheses of the divalent complexes of HPKIH and HPKBH were relatively straightforward. In each case, a charge-neutral divalent 1:2 metal/ligand complex was formed. Charge neutrality occurred through deprotonation of the NH group adjacent to the coordinating imine N atom and carbonyl groups. The pK_a of this group is quite high (>11),[29] but upon coordination of a metal ion, this dropped dramatically, and only deprotonated coordinated ligands were identified here.

The infrared spectra of the complexes have a large number of intense peaks in the range of 1600−1100 cm^{-1}. Despite the systematic variations in metal ion, no obvious trend was seen in the spectra across either the $M(PKIH)_2$ or $M(PKBH)_2$ series, and most bands were almost insensitive to the metal ion present. We tentatively assign the very strong band that appears in the 1485−1500 cm^{-1} range to the coordinated C═O group, which is lowered from the frequency seen in the free ligand of ∼1670 cm^{-1}. Crystallographic data (see below) confirm that the bond order of this carbonyl group is lowered significantly upon coordination of the O atom. The electronic spectra are dominated by transitions common to those of the free ligands. In some cases (notably the Ni and Cu complexes), very weak d−d transitions appeared in the near-infrared region at wavelengths consistent with these metal ions in *cis*-N_4O_2 coordination environments.

Structural Characterization. The crystal structures of a number of complexes from both the $M(PKIH)_2$ and $M(PKBH)_2$ series were determined. Crystallization was facilitated by the fact that most compounds crystallized within one of two isostructural series. Specifically, the series were $[M(PKIH)_2]\cdot nH_2O$ (M = Co, Ni (both $n = 2$), and Cu ($n = 1$)) and $[M(PKBH)_2]\cdot CH_2Cl_2$ (M = Mn, Ni, Cu, and Zn). However, the crystals of $[Cu(PKBH)_2]\cdot CH_2Cl_2$ diffracted quite weakly, and a complete data set was not collected. Instead, upon recrystallization, a solvent-free form of $Cu(PKBH)_2$ was obtained that diffracted much more strongly, and this data set is reported here.

$[M(PKIH)_2]\cdot nH_2O$ (M = Co ($n = 2$), Ni ($n = 2$) and Cu ($n = 1$)). Each complex occupies a general site, as do the solvent molecules. A view of the Co^{II} complex is shown in Figure 2. Although the three compounds are isomorphous, the Cu analogue contained only a single water molecule (disordered over two sites) per complex, whereas two water molecules are found in the Co and Ni structures, each disordered over two sites. This variance does not significantly disrupt the lattice, and the complexes all occupy the same relative positions in their respective structures, but no meaningful discussion of H bonding can be made because of the poor definition of the H atom positions.

The coordination geometries have two meridionally coordinated tridentate (*N*,*N*,*O*) ligands. The M−N and M−O bond lengths (Table 2) show the expected periodic trends and values expected for pyridyl hydrazone complexes of this type.[33] Although the Co and Ni complexes exhibit ap-

(30) Farrugia, L. J. *J. Appl. Crystallogr.* **1999**, *32*, 837.
(31) Sheldrick, G. M. *SHELX97, Programs for Crystal Structure Analysis*; University of Göttingen: Göttingen, Germany, 1997.
(32) Farrugia, L. J. *J. Appl. Crystallogr.* **1997**, *30*, 565.

Table 1. Crystal Data

	$[Co(PKIH)_2]\cdot 2H_2O$	$[Ni(PKIH)_2]\cdot 2H_2O$	$[Cu(PKIH)_2]\cdot H_2O$	$[Mn(PKBH)_2]\cdot CH_2Cl_2$	$[Ni(PKBH)_2]\cdot CH_2Cl_2$	$Cu(PKBH)_2$	$[Zn(PKBH)_2]\cdot CH_2Cl_2$
formula	$C_{34}H_{28}CoN_{10}O_4$	$C_{34}H_{28}N_{10}NiO_4$	$C_{34}H_{26}Cu\ N_{10}O_3$	$C_{37}H_{28}Cl_2MnN_8O_2$	$C_{37}H_{28}Cl_2N_8NiO_2$	$C_{36}H_{26}CuN_8O_2$	$C_{37}H_{28}Cl_2N_8O_2Zn$
fw	699.59	699.37	686.15	742.51	746.28	666.19	752.94
cryst syst	monoclinic	monoclinic	monoclinic	triclinic	triclinic	monoclinic	triclinic
space group	$P2_1/n$	$P2_1/n$	$P2_1/n$	$P\bar{1}$	$P\bar{1}$	$P2_1/n$	$P\bar{1}$
a (Å)	13.785(5)	13.396(3)	13.078(3)	11.734(5)	11.353(4)	10.597(1)	11.477(7)
b (Å)	14.015(2)	14.039(1)	14.339(3)	11.750(4)	11.751(6)	27.450(3)	11.716(4)
c (Å)	17.271(3)	17.571(3)	17.627(2)	14.670(5)	14.698(9)	11.651(2)	14.741(4)
α (deg)				71.84(3)	71.89(5)		71.88(3)
β (deg)	90.58(2)	90.40(2)	92.12(1)	76.68(4)	77.62(5)	109.30(1)	77.58(4)
γ (deg)				64.87(3)	66.64(4)		65.83(3)
V	3337(1)	3304(1)	3303(1)	1729(1)	1702(2)	3198.7(7)	1710(1)
Z	4	4	4	2	2	4	2
D_c	1.393	1.406	1.380	1.427	1.457	1.383	1.462
R_1 (obsd)	0.0562	0.0494	0.0971	0.0756	0.0846	0.0435	0.0937
R_2 (all)	0.1828	0.1574	0.3350	0.2396	0.3305	0.1244	0.3521

Table 2. Selected Bond Lengths (Å), Bond Angles (deg), and Torsional Angles (deg, Absolute Values)

	$[Co(PKIH)_2]\cdot 2H_2O$	$[Ni(PKIH)_2]\cdot 2H_2O$	$[Cu(PKIH)_2]\cdot H_2O$	$[Mn(PKBH)_2]\cdot CH_2Cl_2$	$[Ni(PKBH)_2]\cdot CH_2Cl_2$	$Cu(PKBH)_2$	$[Zn(PKBH)_2]\cdot CH_2Cl_2$
M−N1a	2.019(4)	1.983(3)	1.93(1)	2.202(7)	1.990(7)	1.989(3)	2.06(1)
M−N1b	2.023(4)	1.978(3)	1.96(1)	2.187(6)	1.998(7)	1.947(3)	2.068(9)
M−O1a	2.071(4)	2.070(3)	2.104(8)	2.137(6)	2.073(7)	2.258(3)	2.076(9)
M−O1b	2.088(4)	2.084(3)	2.143(9)	2.128(6)	2.089(6)	2.078(2)	2.091(8)
M−N3a	2.115(4)	2.094(3)	2.13(1)	2.282(8)	2.094(8)	2.254(3)	2.19(1)
M−N3b	2.136(5)	2.098(4)	2.22(1)	2.277(7)	2.093(8)	2.087(3)	2.22(1)
C12a−O1a	1.278(6)	1.269(5)	1.24(1)	1.269(9)	1.26(1)	1.257(4)	1.27(1)
C12b−O1b	1.266(6)	1.275(4)	1.24(1)	1.263(9)	1.28(1)	1.274(4)	1.28(1)
N4a−C12a	1.317(6)	1.340(5)	1.36(2)	1.32(1)	1.34(1)	1.345(4)	1.35(2)
N4b−C12b	1.321(7)	1.330(5)	1.36(2)	1.32(1)	1.35(1)	1.333(4)	1.32(2)
N1a−M−N1b	174.2(2)	176.3(1)	178.6(5)	165.2(3)	173.9(3)	168.7(1)	168.3(4)
N1a−M−O1a	76.4(2)	77.4(1)	78.6(4)	71.9(2)	77.2(3)	74.9(1)	75.8(4)
N1a−M−N3a	76.2(2)	78.0(1)	77.2(5)	71.4(3)	78.3(3)	76.7(1)	74.6(4)
N1a−M−O1b	101.5(2)	101.3(1)	102.7(4)	119.4(2)	107.6(3)	109.5(1)	114.0(4)
N1a−M−N3b	107.1(2)	103.4(1)	104.2(4)	96.5(2)	97.2(3)	93.6(1)	96.1(4)
C7a−C1a−C2a−N2a	51.3(7)	53.7(6)	48(2)	52(1)	48(1)	50.0(4)	51(1)
C7b−C1b−C2b−N2b	53.5(8)	53.3(6)	57(2)	38(1)	33(1)	54.2(5)	38(1)
O1a−C12a−C13a−C17a[a]	8.1(7)	9.1(6)	9(2)	0(1)	0(1)	19.6(5)	0(2)
O1b−C12b−C13b−C17b[a]	16.4(8)	15.6(6)	14(2)	2(1)	2(1)	14.9(6)	0(2)

[a] In the $M(PKBH)_2$ complexes, substitute C17a/b with C14a/b or C18a/b.

proximate 2-fold rotational symmetry, the Cu^{II} complex is exceptional and bears a tetragonally elongated structure with the trans pair of bonds, Cu−N3b and Cu−O1b, being longer than the four remaining bond lengths. This is a consequence of the Jahn Teller effect[34,35] that operates on the d^9 electronic ground state of this six-coordinate complex which elongates one trans pair of coordinate bonds while shortening the remaining four.

In all three structures, the shortest coordinate bonds are to the central imine N donor, while those to the distal pyridyl and carbonyl groups are significantly weaker. This is a superposition of steric and electronic effects. The steric influence may be attributed to the constraints imposed on the central M−N1a/b coordinate bond by the requirement that both O1a/b and N3a/b must also be bound, which in effect enforces a compression of the central coordinate bond. Other meridionally coordinating aromatic tridentate ligands that form consecutive five-membered chelate rings, such as terpyridine, also show this feature.[36−38] The electronic effects relate to a preference for the three metal ions (Co^{II}, Ni^{II}, and Cu^{II}) for N donors over O donors, which augment the above-mentioned steric effect of chelation.

$[M(PKBH)_2]\cdot CH_2Cl_2$ (M = Mn, Ni and Zn) and $Cu(PKBH)_2$. A view of the Zn(II) complex appears in Figure 4. The Mn, Ni, and Zn complexes are isostructural and crystallized with one molecule of dichloromethane per complex, whereas the Cu analogue is a solvent-free form. In the Mn, Ni, and Zn structures, a CH_2Cl_2 molecule donates a nonclassical H bond to one of the free 2-pyridyl N atoms in each structure (C−H···N2a ∼2.44 Å, ∼143°). The trends in M−N and M−O bond lengths mirror those seen in the

(33) Armstrong, C. M.; Bernhardt, P. V.; Chin, P.; Richardson, D. R. *Eur. J. Inorg. Chem.* **2003**, 1145−1146.
(34) Halcrow, M. A. *Dalton Trans.* **2003**, 4375−4384.
(35) Murphy, B.; Hathaway, B. *Coord. Chem. Rev.* **2003**, *243*, 237−262.
(36) Baker, A. T.; Craig, D. C.; Rae, A. D. *Aust. J. Chem.* **1995**, *48*, 1373−1378.
(37) Priimov, G. U.; Moore, P.; Maritim, P. K.; Butalanyi, P. K.; Alcock, N. W. *Dalton Trans.* **2000**, 445−449.
(38) Takusagawa, F.; Yohannes, P. G.; Mertes, K. B. *Inorg. Chim. Acta* **1986**, *114*, 165−169.

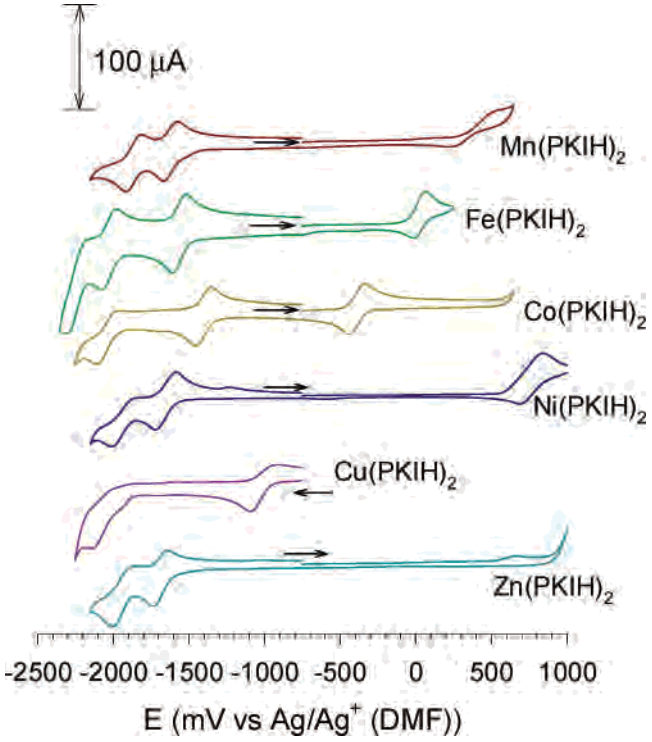

Figure 4. Cyclic voltammograms of the $M(PKIH)_2$ complexes in 100% DMF. The sweep rate was 200 mV/s, and the sweep was initiated in direction of the arrow.

$M(PKIH)_2$ series, and no significant differences were identified. Of note is the fact that, in the Mn^{II} analogue, the Mn−O bonds are shorter than the Mn−N bonds; an electronic effect illustrating the preference for O donors despite the steric constraints imposed on the central Mn−N1a/b bonds.

Angular and Conformational Distortions. The $M(PKBH)_2$ coordination angles are more distorted from an ideal octahedral geometry than the $M(PKIH)_2$ series. For example, the interligand angle N1a−M−O1b is in the range of 107−119° for the PKBH series, but it is around 101° for the three structures from the PKIH series (Table 2). Similarly, the trans N1a−M−N1b angles are much closer to linear in the $M(PKIH)_2$ structures (174−179°) than in the $M(PKBH)_2$ structures (165−174°).

The only conformationally flexible groups in both series are the noncoordinated 2-pyridyl ring and the aromatic substituent on C12 (a phenyl or 4-pyridyl ring). The torsional angles of these groups are given in Table 3, and it is apparent that the 2-pyridyl torsional angles fall in the range of 33−57° (which include 14 independent angles), while the torsional angle of the aromatic substituent attached to the carbonyl group lies in the range of 0−20°. It is apparent that intermolecular interactions within the lattice dictate these torsional angles. The four independent torsional angles given in Table 2 for the three isostructural $[M(PKBH)_2]\cdot CH_2Cl_2$ compounds are the same within experimental error, but they are totally different from those identified in the solvent-free $Cu(PKBH)_2$ and the three isomorphous $[M(PKIH)_2]\cdot nH_2O$ compounds. Given the fact that lattice forces are dictating these dihedral angles, the variations observed going from one lattice to another are actually quite small.

Electrochemistry. Cyclic voltammetry of all complexes was performed in both pure DMF and 50% aqueous DMF. The former solvent allowed a very wide potential range (+0.6 to −2.2 V vs Ag/Ag^+ (DMF)) to be explored. The presence of water limited this range to about +1 to −1 V vs NHE before competitive water oxidation or hydrogen-ion reduction became dominant. These data are presented in Table 3. The results published previously[29] for the Fe^{II} complexes of these ligands (determined under identical conditions) are included here for comparison.

Electrochemistry in 50% Aqueous DMF. The limited aqueous solubility of the complexes necessitated the use of a 1:1 DMF/water mixed solvent. Only the Fe and Co complexes were electroactive within the potential window set by the aqueous solvent mixture, and their $Fe^{III/II}$ and $Co^{III/II}$ redox potentials are given in Table 3. The electrochemistry of the Fe complexes is complicated by reactions of the electrochemically oxidized complex with water leading to a low cathodic/anodic current ratio (an EC mechanism). This mechanism as it applies to these complexes has been described in detail before.[29] In contrast, the $Co(PKIH)_2$ and $Co(PKBH)_2$ complexes exhibit totally reversible $Co^{III/II}$ couples at potentials ca. 500 mV to the negative of the analogous $Fe^{III/II}$ couples. Indeed, the relatively low redox potentials are consistent with our synthetic work which required complexation under an inert atmosphere to minimize oxidation of each complex to its Co^{III} form under refluxing conditions. At room temperature, aerial oxidation is quite slow. Nevertheless, the redox potential of $Co(PKIH)_2$ is ca. 100 mV higher than $Co(PKBH)_2$, and this potential difference permitted the growth of X-ray quality crystals of $Co(PKIH)_2$ over the period of several days in the presence of oxygen where the $Co(PKBH)_2$ complex proved to be more air sensitive in solution and required immediate precipitation to prevent oxidation to its Co^{III} form. The electronic effects of the aromatic substituents on the redox potentials of the complexes is a general feature that has been noted previously with the Fe analogues[29] and relates to the greater electron-withdrawing effect of the 4-pyridyl substituent in each $PKIH^-$ ligand which destablizes the trivalent state relative to the phenyl-substituted $PKBH^-$.

Nonaqueous Electrochemistry (100% DMF). The $M(PKIH)_2$ and $M(PKBH)_2$ (M = Mn, Fe, Co, and Ni) complexes exhibit a reversible or quasi-reversible metal-centered $M^{III/II}$ couple (the highest potential wave in each case) in addition to lower potential waves around −1500 and −2000 mV vs Ag/Ag^+ (Table 3). The voltammograms are illustrated in Figures 4 and 5. The Cu analogues show a quasi-reversible $Cu^{II/I}$ couple and a totally irreversible cathodic wave below −2000 mV. The reversibility of the $Cu^{II/I}$ wave could be enhanced by reversing the sweep before the second irreversible wave is encountered. The Zn complexes show no metal-centered waves, but each exhibits a pair of low-potential waves at similar potentials to that seen for the Mn and Ni analogues.

It is likely that the redox responses seen in the −1400 to −1800 mV range are ligand-centered (radical) reductions. The similarity of the voltammograms in this region across

Table 3. Redox Potentials (mV) as Determined by Cyclic Voltammetry[a]

	$M(PKIH)_2$			$M(PKBH)_2$		
	100% DMF		50% DMF	100% DMF		50% DMF
	metal-centered	ligand-centered	metal-centered	metal-centered	ligand-centered	metal-centered
Mn	+386	−1615, −1869	−	+294	−1743, −1995	−
Fe	+25	−1573, −2050	+606	+30	−1595, −2111	+504
Co	−385	−1403, −2048	+171	−503	−1506, −2178	+47
Ni	+773	−1652, −1932	−	+625	−1801, −2060	−
Cu	−1009	−2064 (irr)	−	−1144	−2219 (irr)	−
Zn	−	−1687, −1938	−	−	−1807, −2012	−
ligand	−	ca. −1.81 (irr)	−	−	ca. −1.97 (irr)	−

[a] Data in DMF cited vs Ag/Ag^+ (DMF) reference. Data in 50% aqueous DMF vs NHE.

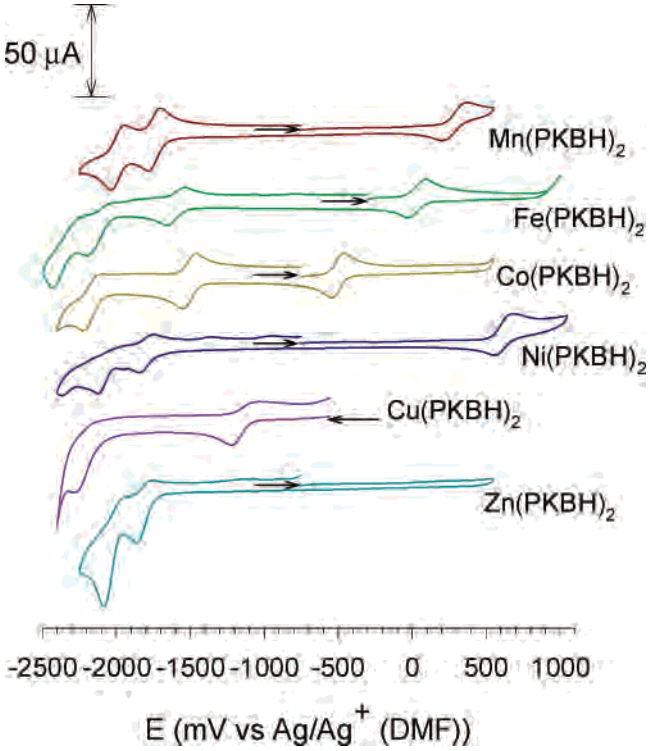

Figure 5. Cyclic voltammograms of the $M(PKBH)_2$ complexes in 100% DMF. The sweep rate was 200 mV/s, and the sweep was initiated in direction of the arrow.

both the $M(PKIH)_2$ and $M(PKBH)_2$ series (which include metals that cannot stabilize six-coordinate monovalent complexes) is strongly suggestive of a ligand-centered reduction. A pyridyl ring is the most likely site of reduction. Conjugated pyridines (such as 2,2′-bipyridyl or 1,10-phenanthroline) are well-known "noninnocent" ligands, and their complexes are capable of undergoing single-electron ligand-centered reductions in preference to metal-centered reductions.[39,40] In the present case, the *coordinated* pyridyl rings of $PKIH^-$ and $PKBH^-$ (as opposed to their noncoordinated aromatic rings) will be the sites that experience the greatest stabilizing influence by the positive charge of the metal ion. The uncomplexed HPKIH ligand yields a totally irreversible cathodic wave at a potential ca. 200 mV negative of the (quasi-)reversible ligand-centered reductions seen in its Mn, Fe, Co, Ni, and Zn complexes. Evidently, the reduction of each free ligand is more difficult than that of its divalent complex, and the product is unstable on the voltammetric time scale. The complexed metal ion offers both thermodynamic and kinetic stability to the ligand radical anion.

The Cu complexes are unique in being unable to achieve this stabilization, and their low-potential irreversible cathodic waves are reminiscent of those found for the free ligands themselves. The reduced monovalent Cu only bears a single positive charge so the thermodynamic stability offered by the divalent analogues (Mn, Fe, Co, Ni, and Zn) will be diminished. Also, a change in coordination geometry on going from six-coordinate Cu^{II} to four-coordinate Cu^{I} is likely, and thus it is possible that one or both pyridyl ligands dissociate from the metal during the voltammetric sweep, losing any stabilizing influence from the metal.

The potentials at which these (quasi-)reversible ligand-centered couples are observed (Figures 4 and 5) vary considerably across the $M(PKIH)_2$ and $M(PKBH)_2$ series. This is interesting and suggests that each metal ion plays its own role (of varying importance) in delocalizing electron density from the reduced ligand radical. The Co complexes appear to offer the greatest stabilizing influence as their $ML^{0/-}$ couples are significantly more positive than the Mn, Fe, Ni, and Zn analogues, which are very similar to each other (Table 3). Six-coordinate Co^{I} complexes are well-known[41] (as opposed to monovalent six-coordinate Mn, Fe, Ni, or Zn complexes), so the additional stability of the $[Co(PKIH)]^-$ compound may well be a consequence of partial electron delocalization of negative charge from the ligand onto the metal in this case. The reversibility of these waves was dependent on the metal ion and the potential at which the sweep was reversed. In each case, if the sweep was reversed immediately following the first ligandcentered reduction, this wave was totally reversible. For example the low anodic/cathodic current ratio of the first ligand-centered couple of $Zn(PKBH)_2$ at −1800 mV is restored to unity if the sweep is reversed at −1900 mV (data not shown).

Additional responses were seen in the −1900 to −2100 mV range. The reversibility and current maxima varied across this series. The Mn, Fe, and Zn complexes of both series exhibited reversible low-potential one-electron waves, whereas the Co and Ni complexes gave irreversible waves that were

(39) Puntoriero, F.; Serroni, S.; Galletta, M.; Juris, A.; Licciardello, A.; Chiorboli, C.; Campagna, S.; Scandola, F. *ChemPhysChem* **2005**, *6*, 129−138.
(40) Bassani Dario, M.; Lehn, J.-M.; Serroni, S.; Puntoriero, F.; Campagna, S. *Chem.−Eur. J.* **2003**, *9*, 5936−5946.
(41) Bernhardt, P. V.; Lawrance, G. A. *Compr. Coord. Chem. II* **2004**, *6*, 1−145.

Table 4. Antiproliferative Activity of HPKIH, HPKBH, and Their Divalent Transition Metal Complexes after a 96 h Incubation with SK-N-MC Neuroepithelioma Cells[a]

chelators/complexes	IC_{50} (μM)	*p*
DFO	18.59 ± 5.36	–
DOX	0.04 ± 0.13	–
HPKIH	0.96 ± 0.23	–
$Mn(PKIH)_2$	0.64 ± 0.14	< 0.18 (NS)
$Fe(PKIH)_2$	0.32 ± 0.06	< 0.005
$Co(PKIH)_2$	1.07 ± 0.40	< 0.65 (NS)
$Ni(PKIH)_2$	0.60 ± 0.19	< 0.17 (NS)
$Cu(PKIH)_2$	0.46 ± 0.17	< 0.013
$Zn(PKIH)_2$	0.48 ± 0.23	< 0.02
HPKBH	3.57 ± 0.33	–
$Mn(PKBH)_2$	0.46 ± 0.05	< 0.0003
$Fe(PKBH)_2$	0.57 ± 0.35	< 0.006
$Co(PKBH)_2$	0.50 ± 0.24	< 0.0009
$Ni(PKBH)_2$	1.27 ± 0.11	< 0.0235
$Cu(PKBH)_2$	0.90 ± 0.15	< 0.003
$Zn(PKBH)_2$	0.54 ± 0.17	< 0.0006

[a] Proliferation was determined by the MTT assay (see Experimental Section for further details). Results are mean ± SD (4 experiments). The *p* values were determined using Student's *t*-test, and the activity of the ligand was compared to its relevant complex. A value of $p > 0.05$ was considered as not significant (NS).

~1.4 times greater than those of the single-electron waves. This indicates that more than one electron is involved in this reaction, but the current is less than that expected[42] for a cooperative 2-electron process. (The current maximum of an *n*-electrovoltammetric wave is proportional to $n^{3/2}$; thus if the electron-transfer rate constants of the two waves are similar, a two-electron wave will appear 2.83 times greater than a one-electron wave.) The responses were also irreversible, and this compromised the reversibility of the higher potential couples in some cases. Like the waves seen in the −1400 to −1600 mV region, the low-potential couple is most probably associated with ligand-centered reduction, but given the complexity of these responses, further speculation on their origin is not offered.

Antiproliferative Activities of HPKIH, HPKBH, and Their Divalent Complexes. Previous studies have demonstrated that complexation of aroylhydrazone chelators with metal ions can result in marked alterations in the biological activity of these compounds.[12,43,44] To assess the effect of complexation on antiproliferative activity, two series of divalent transition metal complexes, $M(PKIH)_2$ and $M(PKBH)_2$ (M = Mn, Fe, Co, Ni, Cu, and Zn), were examined (Table 4). In the present studies, two relevant positive controls were also screened, namely, the clinically used Fe chelator, desferrioxamine (DFO), and the widely used antitumor agent, doxorubicin (DOX). Desferrioxamine shows relatively low antiproliferative activity against SK-N-MC neuroepithelioma cells ($IC_{50} = 19 \pm 5$ μM), while DOX shows marked efficacy ($IC_{50} = 0.04 \pm 0.1$ μM). The results for the two series are summarized in Table 4 with their standard deviations indicated. Both HPKIH and HPKBH were less effective antiproliferative agents than DOX, but they were far more effective than DFO, having IC_{50} values of 0.96 μM and 3.57 μM, respectively.

Complexation of the chelators with the divalent transition metals Mn, Fe, Co, Ni, Cu, and Zn had variable effects depending upon whether the $M(PKIH)_2$ or $M(PKBH)_2$ complexes were assessed (Table 4). In the case of the $M(PKIH)_2$ series, the Fe, Cu, and Zn complexes were significantly ($p < 0.02$) more effective than the free ligand. Complexation of HPKIH with Mn, Co, and Ni gave no significant ($p > 0.05$) enhancement or decrease in antiproliferative activity. By contrast, the antiproliferative effect of HPKBH was significantly ($p < 0.02$) enhanced upon complexation with each of the six metal ions examined herein. This should be viewed in perspective, as the IC_{50} value of HPKBH is more than three times higher than that of HPKIH (Table 4). The important point is that although the activities of the two free ligands are significantly ($p < 0.005$) different, upon complexation, the antiproliferative efficacy of the two series converge to values that are rather similar.

Several trends that may be important for the future design of these compounds and their medical applications were apparent from the data comparing the transition metal complexes and their ligands. In both HPKIH and HPKBH, complexation with a divalent transition metal either enhanced or had no effect on the already pronounced antiproliferative activity of each chelator (Table 4). This behavior may be contrasted with that seen for the highly cytotoxic ligand, H_2-NIH, which loses all antiproliferative activity if complexed with Fe^{III} prior to incubation with cells.

The increased antiproliferative activity of some of the complexes compared to their relevant ligands could be the result of a combination of factors. First, complexation of HPKIH and HPKBH with a metal ion may facilitate their passage across cell membranes. Upon complexation, the donor atoms of each ligand become inaccessible to solvent, and the NH proton is lost. This may result in a more lipophilic compound[45] which can better penetrate cellular compartments that are linked to cellular proliferation. In fact, our previous studies have clearly demonstrated that there is a good correlation between antiproliferative activity and lipophilicity of tridentate aroylhydrazone ligands.[12] In the case of the Fe^{II} complex, facile entrance into the cell of this redox-active species may enable greater antiproliferative activity because of the generation of toxic free radicals that damage vital biomolecules such as DNA and proteins.[14,18,29] However, the most significant finding of this study is that the redox-active complexes of Fe^{II} and Co^{II} are no more active than complexes that are redox inactive in water (e.g., Zn^{II} or Mn^{II}, Table 4).

These latter observations now raise the possibility of a second factor which could increase the antiproliferative effect of the chelator over the complex. That is, the complexes may act as lipophilic transport vehicles that donate a toxic metal

(42) Bard, A. J.; Faulkner, L. R. *Electrochemical Methods: Fundamentals and Applications*, 2nd ed.; Wiley: New York, 2001.
(43) Johnson, D. K.; Murphy, T. B.; Rose, N. J.; Goodwin, W. H.; Pickart, L. *Inorg. Chim. Acta* **1982**, *67*, 159−165.
(44) Richardson, D. R. *Antimicrob. Agents Chemother.* **1997**, *41*, 2061−2063.
(45) Edward, J. T.; Ponka, P.; Richardson, D. R. *BioMetals* **1995**, *8*, 209−217.

ion to an inappropriate cellular acceptor molecule which then leads to inhibition of growth. It has been known for some time that the antiproliferative effects of metal complexes of some cytotoxic chelators are greater than those of their free ligands.[43,46,47] A specific example is the related hydrazone ligand, H_2PIH, which shows very little antiproliferative activity.[12,44] However, upon complexation of H_2PIH with Ga^{III}, its antiproliferative activity increases to an extent greater than that found for the ligand or uncomplexed Ga^{III} alone.[12,44] This is probably caused by the ability of the Ga^{III} complex to donate free Ga^{III} to the cell after internalization.[12] Because of the similarity of Ga^{III} and Fe^{III}, Ga acts to replace Fe in the active sites of the rate-limiting enzyme of DNA synthesis, ribonucleotide reductase. This effect of the donated Ga leads, at least in part, to its antitumor effects.[48] Furthermore, previous studies have demonstrated that some aroylhydrazone Fe complexes are capable of acting as Fe donors to cells,[49,50] confirming the ability of such metal complexes to act as lipophilic transport and delivery shuttles. The formation of a complex which shows greater lipophilicity than the ligand may permit greater entrance into the cell which is then followed by dissociation of the ligand and metal ion. The chelator can then act to induce its effects via binding Fe to deprive essential metabolic pathways of this vital metal ionor the Fe complex can engage in redox cycling to generate cytotoxic free radicals that damage biomolecules. For HPKIH and HPKBH, previous studies have demonstrated that both of these latter mechanisms are feasible.[18,28,29]

The complexes of some of the ligands prepared in the current investigation may be suitable for further assessment of their antiproliferative activity in animal models.[17] Certainly, it would be of interest to determine if the complexes (as opposed to the ligands) show greater selectivity against tumors compared to their effect on normal tissues.

Conclusions

Importantly, we have demonstrated that redox-inactive complexes of both HPKIH and HPKBH exhibit antiproliferative activity that is similar or greater than that of the free ligands. If redox activity is indeed important in the antiproliferative activity of the Fe^{II} complexes of these ligands, then it cannot be the only mechanism by which these ligands and complexes exert their antitumor effects. We suggest that the complexes act as lipophilic transport shuttles that allow entrance to the cell and enable the delivery of both the ligand and metal which act in concert to inhibit proliferation. Further work will be needed to better understand the manner in which these complexes interact with the molecules that regulate cellular proliferation; this is currently underway.

Acknowledgment. P.V.B. and D.R.R. gratefully acknowledge support from the Australian Research Council (DP0450001). D.R.R. acknowledges Fellowship and Project Grant support from the National Health and Medical Research Council of Australia in addition to the National Ataxia Foundation USA and the Muscular Dystrophy Association USA for grant support. We also sincerely thank Dr. Jonathan Howard for technical assistance. Children's Cancer Institute Australia for Medical Research is affiliated with the University of New South Wales and Sydney Children's Hospital.

Supporting Information Available: Crystallographic data in CIF format. This material is available free of charge via the Internet at http://pubs.acs.org.

IC051573L

(46) Booth, B. A.; Donnelly, T. E., Jr.; Zettner, A.; Sartorelli, A. C. *Biochem. Pharmacol.* **1971**, *20*, 3109−3118.
(47) Graham, R. D.; Williams, D. R. *J. Inorg. Nucl. Chem.* **1979**, *41*, 1245−1249.
(48) Chitambar, C. R.; Matthaeus, W. G.; Antholine, W. E.; Graff, K.; O'Brien, W. J. *Blood* **1988**, *72*, 1930−1936.
(49) Ponka, P.; Schulman, H. M. *J. Biol. Chem.* **1985**, *260*, 14717−14721.
(50) Ponka, P.; Schulman, H. M.; Wilczynska, A. *Biochim. Biophys. Acta* **1982**, *718*, 151−156.